applied sciences

MDPI

Article

Enzymatic Analysis of Chitin Deacetylases on Crystalline Chitin with Varied Molecular Weights: Insights from Active Pocket Characteristic Analysis

Kaige Chen, Shengyu Yang and Jun Cai *

School of Life and Health Sciences, Hubei University of Technology, Wuhan 430000, China; kaige_0227@163.com (K.C.)
* Correspondence: hgdcaijun@hbut.edu.cn; Tel.: +86-18971544678

Abstract

Chitin deacetylases (CDAs), which catalyze the deacetylation of chitin to produce chitosan, have garnered significant interest due to their environmental compatibility and ability to control product quality. However, the low conversion efficiency resulting from chitin's high molecular weight and crystallinity, as well as structural limitations of CDAs, has impeded their industrial application. In this study, we present the integrated approach combining bioinformatics and computational tools (adaptive Poisson–Boltzmann solver, Fpocket, and ProteinPlus) to systematically analyze sequence features and variations in active pocket properties among CDAs from diverse origins. Experimental evaluation of the deacetylation activity of *An*CDA, *As*CDA, *Ba*CDA, and *Sc*CDA, each with distinct pocket characteristics, on chitin substrates with varying molecular parameters revealed that CDAs with high hydrophobicity scores and low surface-to-volume ratios exhibited superior efficiency in converting high-molecular-weight chitin. These findings guide the rational selection and engineering of CDAs for industrial biocatalysis.

Keywords: chitin deacetylase; active pocket; crystalline chitin; enzymatic reaction; heterologously expressed

check for updates

Academic Editor: Maria Annunziata M. Capozzi

Received: 18 September 2025
Revised: 1 October 2025
Accepted: 2 October 2025
Published: 5 October 2025

Citation: Chen, K.; Yang, S.; Cai, J. Enzymatic Analysis of Chitin Deacetylases on Crystalline Chitin with Varied Molecular Weights: Insights from Active Pocket Characteristic Analysis. *Appl. Sci.* **2025**, *15*, 10721. https://doi.org/10.3390/app151910721

Copyright: © 2025 by the authors. Licensee MDPI, Basel, Switzerland. This article is an open access article distributed under the terms and conditions of the Creative Commons Attribution (CC BY) license (https://creativecommons.org/licenses/by/4.0/).

1. Introduction

Chitosan, a key derivative obtained through the partial deacetylation of chitin, exhibits significantly improved properties than chitin, whose high crystallinity limits its solubility [1,2]. The lower molecular weight, reduced crystallinity, and increased density of free amino groups confer notable advantages to chitosan, in terms of solubility and potential for functional modification [3,4], thereby facilitating its widespread industrial application [5,6]. Despite the industrial use of traditional chemical methods involving high-concentration sodium hydroxide-mediated deacetylation at elevated temperatures, these approaches face critical challenges, including severe environmental pollution, high energy consumption, and inconsistent product quality [7–11]. Enzymatic strategies for chitosan preparation are emerging as promising approaches for sustainable biomanufacturing, owing to their mild reaction conditions, reduced energy consumption, and improved product quality consistency [12,13].

Chitin deacetylase (CDA), a key enzyme that catalyzes the direct deacetylation of chitin, has been identified in a wide range of organisms, including bacteria, fungi, arthropods, protozoa, and algae [14]. Although substantial efforts have been made to explore

the physiology of CDAs, such as strain screening, heterologous expression, and analysis of deacetylation patterns [15,16], most studies primarily focus on chitin oligomers as substrates. It is also worth noting that research on the domains of CDA family members with chitin-catalytic activity is currently inadequate, and their structure-activity relationships need further investigation. The high molecular weight and high crystallinity of chitin, along with limitations in the structural characteristics of CDAs themselves, result in low chitin conversion efficiency, which is unfavorable for the industrial enzymatic production of chitosan [17,18].

From a molecular perspective, substrate specificity in CDAs is closely associated with their structural characteristics [19]. All members of the carbohydrate esterase 4 (CE4) family possess a NodB homologous domain, with five conserved motifs (MT1–MT5) within the catalytic pocket (Figure 1). In particular, MT1 (TF/YDD) and MT2 (H[S/T]xxH) cooperate via aspartate and histidine residues to form a metal ion–binding histidine–histidine–aspartate (His–His–Asp) triad essential for metal-dependent catalysis [20,21]. Additionally, the MT3 (RxP[Y/F][L/F/G]) and MT4 (DxxD[W/Y]) motifs form a structurally symmetric groove that frequently enhances substrate binding through hydrophobic residues such as phenylalanine or leucine. In contrast, MT5 ([V/I]L/F/YxHD) serves a dual function in catalysis and in modulating the hydrophobic environment of the active site [19]. The precise arrangement and interactions of these structural elements determine the hydrophobicity, charge distribution, and spatial dimensions of the active site, which in turn affect substrate-binding affinity and catalytic efficiency [22–25].

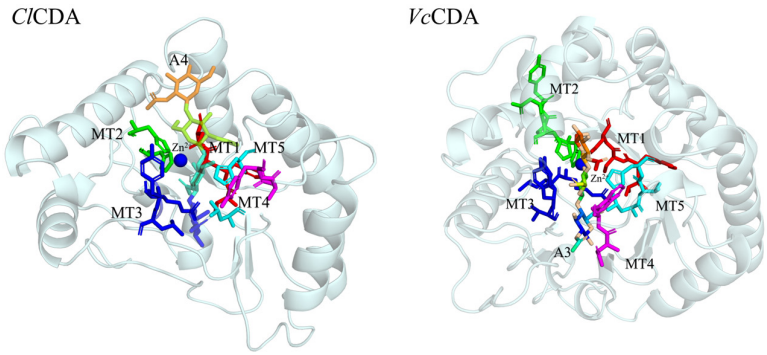


Figure 1. Spatial position of conserved motifs MT1–MT5 in the catalytic domain of *Cl*CDA and *Vc*CDA. *Cl*CDA: the chitin deacetylase from *Colletotrichum lindemuthianum.* *Vc*CDA: the chitin deacetylase from *Vibrio cholerae.* The five conserved motifs (MT1-5) were colored.

To date, only a limited number of studies have examined the effects of active-site engineering on CDA performance, with the majority of research focusing on chitin oligomer catalysis. Systematic investigations into the deacetylation of chitin substrates with varying molecular properties are still lacking. To achieve the efficient conversion of chitin and high-quality production of chitosan, it is essential to deepen research on the structure of CDAs. By comparing the structures of CDAs from different origins with different catalytic efficiencies and identifying potential common structural features, this will provide a theoretical basis for modifying CDAs via protein engineering approaches to enhance their catalytic efficiency. This study employed computational tools to analyze the microenvironmental properties of active sites across various CDAs, including charge distribution, hydrophobicity, and surface-to-volume (S/V) ratio, thereby identifying candidate sequences with significant structural divergence. Selected enzymes were heterologously expressed in *Escherichia coli* as soluble recombinant proteins, purified using nickel-affinity chromatography, and assessed for their deacetylation efficiency on chitin substrates with varying molecular parameters. These

findings provide a theoretical foundation for engineering CDAs via protein engineering strategies aimed at enhancing catalytic performance for industrial applications.

2. Materials and Methods

2.1. Materials

The amino acid sequences of *An*CDA (GenBank: EAA66447.1), *As*CDA (GenBank: MW295944.1), *Ba*CDA (GenBank: WP_013054966.1), and *Sc*CDA (GenBank: NP_013411.1) were retrieved from the NCBI database (https://www.ncbi.nlm.nih.gov/, accessed on 23 May 2024). Signal peptides and non-essential regions were removed, and the resulting coding sequences were codon-optimized prior to gene synthesis by Sangon Biotech (Shanghai, China). Competent *E. coli* strains BL21 and DH5α were obtained from Weidi Biotech (Shanghai, China). Kanamycin (50 μg/mL), isopropyl β-D-1-thiogalactopyranoside (IPTG), a plasmid miniprep purification kit, and protein quantification assay kits were acquired from Sangon Biotech (Shanghai, China). Chitin and chitosan substrates were obtained from Shanghai Macklin Biochemical Co., Ltd. (Shanghai, China). All chemical substances used were of analytical grade.

2.2. Phylogenetic Analysis and Active-Site Characterization of CDAs

CDA sequences known to act on substrates such as ethylene glycol chitin, colloidal chitin, and crystalline chitin were retrieved from the NCBI database (https://www.ncbi.nlm.nih.gov/, accessed on 23 May 2024; a complete list of accession numbers is provided in Table 1). Signal peptides and redundant regions were removed to retain only the full-length catalytic domains. Multiple sequence alignment was performed using Jalview 2.11.2 [26]. Phylogenetic analysis was conducted using the maximum likelihood method in MEGA version 7 with 1000 bootstrap replicates [27]. Given the scarcity of experimentally resolved CDA crystal structures, protein structure prediction was employed. Three-dimensional models of CDAs were generated using AlphaFold3 (https://alphafoldserver.com/, accessed on 17 July 2024), evaluated for quality with SEVES version 6.1 (https://saves.mbi.ucla.edu/, accessed on 2 August 2024), and the highest-scoring models were processed using PyMOL version 3.1 (https://pymol.org/, accessed on 10 August 2024) [28]. Electrostatic surface potentials were calculated using the adaptive Poisson-Boltzmann solver (APBS) plugin, and hydrophobicity analysis was performed using the built-in PyMOL algorithm [29]. Finally, active sites of CDAs were compared in terms of hydrophobicity scores, volume, and solvent-accessible surface area using Fpocket (https://durrantlab.pitt.edu/fpocketweb/, accessed on 19 September 2024) and Protein-Plus (https://proteins.plus/, accessed on 22 September 2024) to identify CDAs with distinct structural characteristics [30,31].

Table 1. Gene list used in this study.

Source of Strain	GenBank Accession Numbers	Name	Source of Strain	GenBank Accession Numbers	Name
Acinetobacter schindleri	MW295944.1	*As*CDA	*Pestalotiopsis* sp.	A0A1L3THR9	*Pes*CDA
Bacillus licheniformis	Q65LW7	*Bl*CDA	*Rhizopus nigricans*	AY779045	*Rn*CDA
Bacillus aryabhattai TCI-16	WP_028412810.1	*Bat*CDA	*Mucor rouxii*	P50325	*Mr*CDA
Aspergillus nidulans FGSC A4	Q5AQQ0	*An*CDA	*Colletotrichum lindemuthianum*	Q6DWK3	*Cl*CDA
Bacillus aryabhattai B8W22	WP_028412720.1	*Ba*CDA	*Podospora anserina*	B2AAQ0	*Pa*CDA
Arthrobacter	5LFZ	*Ar*CE4	*Rhizopus circinans*	A0A9P6XCG4	*Rc*CDA
Arthrobacter sp. Jub115	WP_133834943	*Ar*CDA	*Rhizopus stolonifer*	A0A367KRZ9	*Rs*CDA
Coprinopsis cinerea	A8P2Z0	*Cc*CDA	*Streptomyces bacillaris*	WP_112490308	*Sb*CDA

Table 1. *Cont.*

Source of Strain	GenBank Accession Numbers	Name	Source of Strain	GenBank Accession Numbers	Name
Flammulina velutipes	BAE92728	*Fv*CDA	*Streptomyces griseoinacarnatus* RB7AG	QFX82172	*Sg*CDA
Aspergillus flavus	Q2UI04	*Af*CDA	*Saccharomyces cerevisiae* S288C	Q06703	*Sc*CDA
Puccinia striiformis f. sp. *tritici*	A0A0L0W1E0	*Pgt*CDA	*Aspergillus niger*	A2QZC8	*Ang*CDA

2.3. Heterologous Expression and Purification of Recombinant CDAs

Codon-optimized genes *An*CDA, *As*CDA, *Ba*CDA, and *Sc*CDA were directionally cloned into the pET-28a(+) expression vector using BamHI and XhoI restriction sites. The recombinant plasmids were transformed into competent *E. coli* BL21(DE3) cells via heat shock. Transformants were inoculated into Luria–Bertani (LB) broth supplemented with 50 μg/mL kanamycin and incubated at 37 °C with shaking at 220 rpm until an optical density at 600 nm (OD_{600}) of 0.6–0.8 was reached. Protein expression was induced by the addition of 0.2 mM IPTG, followed by incubation at 20 °C for 16 h with agitation reduced to 200 rpm. Recombinant proteins were purified using a protein purification system (Bio-Rad, USA) equipped with a nickel–nitrilotriacetic acid resin column. Analysis of the crude lysates, along with the wash and elution fractions, was performed by subjecting the proteins to separation on 12% SDS–polyacrylamide gels under reducing conditions.

2.4. Enzyme Assay of CDAs

The enzymatic activity of the recombinant CDAs was determined with p-nitroacetanilide as the substrate. [32]. The reaction mixture consisted of 0.1 mL of recombinant CDA, 0.1 mL of a 200 mg/L *p*-nitroacetanilide solution, and 0.3 mL of phosphate buffer (pH 7.4). The mixture was incubated at 37 °C for 30 min, followed by termination of the reaction by boiling in a water bath for 10 min. A blank control was prepared using an equivalent concentration of heat-inactivated enzyme under otherwise identical conditions. Absorbance was measured at 400 nm, and enzyme activity was calculated accordingly. One unit of enzyme activity was defined as the amount of enzyme required to release 1 μg of *p*-nitroaniline per hour under the specified assay conditions.

2.5. Optimization of Reaction Conditions for Recombinant Proteins

A systematic analysis of temperature and pH influence was conducted to establish the optimal reaction parameters for the recombinant CDAs. Thermostability was assessed by incubating the purified enzymes (*As*CDA, *An*CDA, *Ba*CDA, and *Sc*CDA) at different temperatures. At scheduled intervals (0–12 h), samples were retrieved, and the reaction was quenched by boiling for 10 min before activity assay. The activity recorded at the 0 h time point for each temperature was used as the baseline (100%) for calculating relative activities thereafter. The pH optimum was determined following a 2 h incubation of the enzyme solutions in various pH buffers at 4 °C. After similar heat inactivation, the pH condition yielding the peak activity was assigned a value of 100%, against which all other relative activities were normalized.

2.6. Catalytic Performance on Chitin Substrates

Commercial chitin was dispersed in 10%, 20%, and 30% (*w*/*v*) sodium hydroxide solutions at a solid-to-liquid ratio of 1:20 (g/mL) to create chitin–alkali composite systems. These systems were subjected to gradient ultrasonication at power levels of 400 W and 600 W under room temperature or ice-bath conditions, for treatment durations ranging

from 10 to 60 min at 10 min intervals [33]. After each treatment, the reaction mixtures were neutralized, washed with deionized water, and freeze-dried to obtain 7 distinct chitin substrates (designated a–g).

Forty milligrams of each varied molecular weight chitin substrate was dispersed in 50 mM phosphate buffer. Recombinant chitin deacetylase (30 U) was added to each mixture, and reactions were carried out under optimal conditions for 12 h with continuous stirring. The enzymatic reactions were terminated by placing the mixture in a boiling water bath, followed by washing with deionized water and freeze-drying to obtain the deacetylated products. Fourier transform infrared spectroscopy (FT-IR) was employed to quantitatively analyze the characteristic shifts in acetyl group peaks. The degree of deacetylation (DD%) was calculated using a standard curve to evaluate the catalytic specificity of the enzyme toward substrates of different molecular weights.

2.7. Substrate Characterization

2.7.1. Molecular Weight Determination of Substrates

The intrinsic viscosities of commercial chitin and substrates a–g were measured using an Ubbelohde viscometer (capillary diameter: 0.58 mm; Zhejiang glass instrument factory, Bao Yang County, Jiangsu Province, China). Samples were dissolved in a 5% lithium chloride (LiCl)/*N*,*N*-dimethylacetamide (DMAC) solution, and both relative viscosity and intrinsic viscosity ([η]) were calculated based on the flow times of the sample solution and the pure solvent. The viscosity-average molecular weight (M_w) of chitin was then determined using the Mark–Houwink–Sakurada equation [34]:

$$[\eta] = KM_w^{\alpha} \quad (1)$$

where $K = 7.6 \times 10^{-5}$ and $\alpha = 0.95$ are constants.

2.7.2. FT-IR Analysis

FT-IR analysis was conducted on substrates both before and after enzymatic catalysis using a Nicolet iS10 spectrometer (Thermo Fisher Scientific, Waltham, MA, USA). Spectra were recorded over the range of 500–4000 cm^{-1} at a resolution of 4 cm^{-1}. The degree of deacetylation (*DD*%) was calculated by analyzing the intensities of the characteristic absorption peaks using the following formula [35]:

$$DD(\%) = (1 - \frac{\frac{A_{1320}}{A_{1420}} - 0.3822}{0.03133}) \times 100 \quad (2)$$

where A_{1320} and A_{1420} represent the absorbance intensities at 1320 cm^{-1} (Amide III band (C–N stretching + N–H bending)) and 1420 cm^{-1} (the $–CH_2$ bending vibration), respectively. The numbers 0.3822 and 0.03133 are the fitting parameters of the linear calibration equation.

2.7.3. X-Ray Diffraction (XRD) Analysis

Commercial chitin, chitosan, and substrates a–n were analyzed for crystallinity using a Miniflex 600 X-ray diffractometer (Rigaku, Tokyo, Japan) with a 2θ scanning range of 5–45° at a scanning speed of 5°·min^{-1}. The crystallinity index (*CrI*) of the samples was calculated using the following equation [36]:

$$CrI = \frac{I_{110} - I_{am}}{I_{110}} \times 100\% \quad (3)$$

where I_{110} and I_{am} represent the diffraction intensities at approximately $2\theta \approx 20°$ and $2\theta \approx 16°$, respectively.

2.8. Statistical Analysis

Each experiment was conducted in biological triplicates. The data represents the mean value of the three parallel experiments, and the corresponding standard deviations are indicated by error bars.

3. Results and Discussion

3.1. Bioinformatics Analysis of CDAs

3.1.1. Phylogenetic Analysis and Multiple Sequence Alignment

We conducted phylogenetic and sequence alignment analyses on 22 CDAs reported in the literature, which utilize ethylene glycol chitin, colloidal chitin or chitin as substrates (Figures 2 and 3). The phylogenetic tree revealed that fungal and bacterial CDAs formed distinct clades, suggesting significant evolutionary divergence likely influenced by variations in host organisms and environmental conditions. Fungal CDAs were further categorized into two subgroups. The first subgroup is primarily associated with host infection; for example, *Pgt*CDA, secreted by *Puccinia graminis f.* sp. *tritici* (wheat rust), plays a crucial role in infection and colonization by counteracting the hydrolysis of fungal cell wall chitin by host-derived chitinases [37]. The second subgroup primarily contributes to cell wall formation, as demonstrated by *Sc*CDA, which is involved in the development of the ascospore wall in *Saccharomyces cerevisiae*, and *Mr*CDA from *Mucor rouxii,* which participates in cell wall construction [38,39]. In contrast, bacterial CDAs exhibited an independent branch in the phylogenetic tree, comprising several subgroups with notable sequence variability. This heterogeneity suggests that, during long-term adaptation to changing environments, these enzymes may have undergone evolutionary diversification. These adaptations may have led to the expansion and optimization of catalytic and substrate-binding function [40]. Furthermore, bacterial CDAs have been shown to rapidly respond to fluctuations in substrate and metal ion concentrations in their surroundings, thereby playing critical roles in symbiosis, nutrition acquisition, and metabolic regulation [14,41,42]. For example, *Ar*CE4, secreted by a *Jeotgalibacillus* sp., is believed to utilize environmental chitin as a crucial nutrient source [43].

Multiple sequence alignment analysis (Figure 3) revealed that the catalytic motifs MT1–MT5 are more highly conserved in fungal CDAs, a characteristic likely associated with the necessity for efficient chitin processing during cell wall remodeling [17,22,44,45]. Although most bacterial CDAs retain these core motifs, significant differences were observed in the MT1–MT5 regions of *As*CDA and *Ba*CDA. In *As*CDA, the canonical Asp–His–His metal-binding triad is replaced by Glu–His–Trp. *Ba*CDA exhibits similar non-conservative substitutions in MT1 (TFNI) and MT2 (MxxxY), although it retains the catalytic histidine residue in MT5. These conserved motifs define the active site and substrate-binding pocket, thereby influencing CDA catalytic mechanism. Substrates with varying molecular weights display distinct binding geometries and steric hindrances. Bacterial CDAs may exploit motif variations to enhance the active-site flexibility, allowing adaptation to substrates with differing physicochemical properties such as crystallinity and polymer chain length [43,46,47]. Phylogenetic clustering places *As*CDA and *Ba*CDA within the single clade, characterized by divergent motif evolution, indicating that these enzymes have experienced structural diversification that may underlie variations in catalytic efficiency and substrate specificity. *As*CDA has been reported to exhibit high catalytic activity against α-chitin [46]. Although the deacetylation of crystalline chitin by *Ba*CDA has not yet been characterized, its sustained activity under high ionic strength and its effectiveness against ethylene glycol chitin derivatives suggest an environmentally adaptive role that may facilitate chitin degradation [18,41].

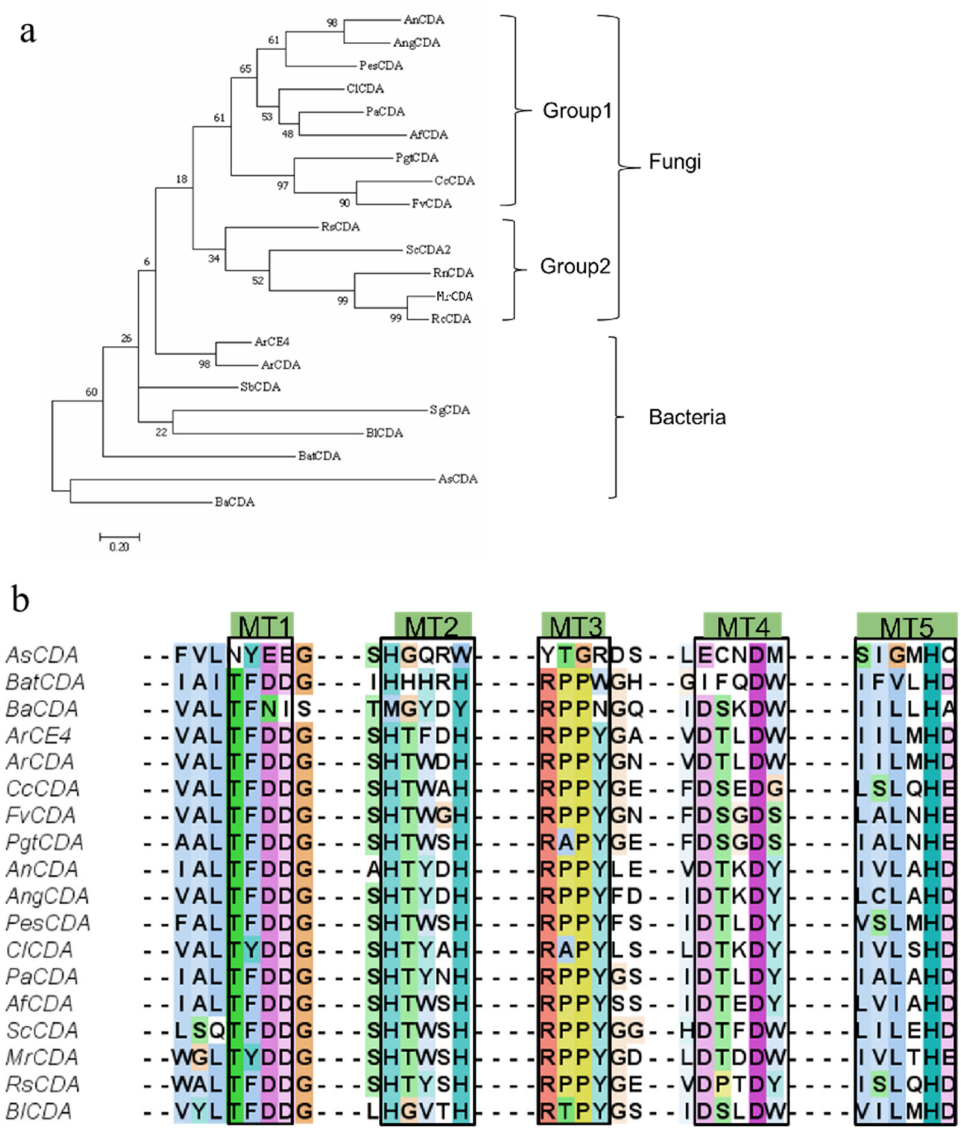


Figure 2. (**a**) Phylogenetic tree of chitin deacetylases (CDAs) from fungal and bacterial sources constructed using neighbor-joining analysis, with bootstrap values indicated at branch points. (**b**) Multiple sequence alignment of conserved motifs (MT1–MT5) in representative CDA sequences.

3.1.2. Charge Distribution and Geometric Parameters of the Active Pocket

We calculated the surface electrostatic potentials of the enzyme active sites using the APBS plugin (Figure 3a).

In most CDAs, the MT1–MT5 regions are enriched with negatively charged amino acid residues, primarily aspartic acid (Asp) and glutamic acid (Glu), creating an electrostatic environment conducive to attracting positively charged substrates, such as glucosamine (GlcN). This observation aligns with the deacetylation mechanism proposed for *Saccharomyces cerevisiae* [48].

Conversely, catalytic pockets with net positive electrostatic potentials seem to promote binding of N-acetylglucosamine moieties [49]. *Ba*CDA exhibits a heterogeneous charge distribution, due to the incorporation of neutral or positively charged residues, such as arginine (Arg), within its conserved motifs (Figure 3b). This mixed electrostatic landscape may confer substrate specificity toward chitin oligosaccharides with defined degrees of polymerization or varying states of partial acetylation [18].

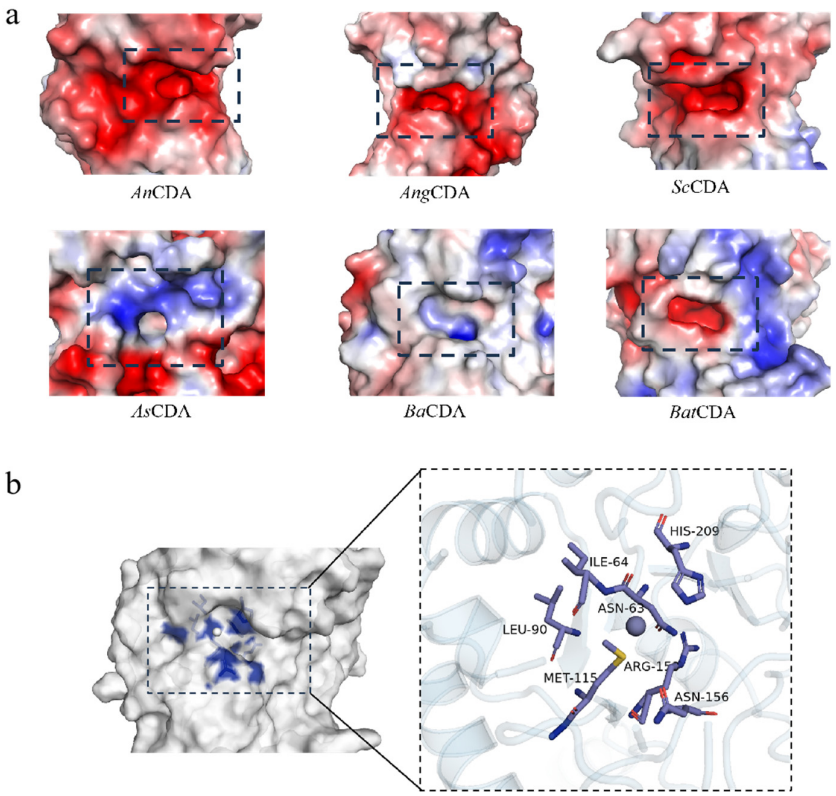


Figure 3. (**a**) Electrostatic surface potential distributions of selected CDAs. The distribution of surface charge is illustrated as follows: red regions represent negative charges, blue regions indicate positive charges, and white regions denote neutral charges. The active pocket is highlighted within a dashed black box. (**b**) Structural details of the catalytic pocket of *Ba*CDA. Key amino acid residues are shown in stick representation. The catalytic site is magnified in the right panel.

In terms of geometric parameters, computational analysis using ProteinPlus and Fpocket revealed that the active pockets of CDAs generally exhibit surface areas ranging from 150 to 400 Å^2 and volumes between 100 and 200 Å^3, with notable variations in hydrophobicity scores (Table 2).

Larger volumes and surface areas typically indicate more spacious active pockets capable of accommodating bulkier or structurally complex substrates, whereas smaller dimensions suggest compact pockets that may enhance substrate selectivity. A high volume-to-surface area ratio implies deep, narrow pocket conformations, while a low ratio corresponds to shallow, open architectures that facilitate rapid substrate release [50,51].

Correlation analysis of pocket physicochemical properties and catalytic performance revealed the following trends (Table 2): (1) CDAs with low hydrophobic scores and high surface-to-volume ratios (S/V > 2.4) preferentially catalyzed oligomeric chitin but exhibited poor activity toward crystalline chitin; (2) Enzymes that combine high hydrophobicity with elevated S/V ratios (>2.4) or low hydrophobicity with reduced S/V ratios (<2.4), demonstrated minimal activity toward crystalline chitin; (3) CDAs with high hydrophobicity and low S/V ratios (<2.4) displayed measurable catalytic efficiency toward crystalline chitin. The deacetylation activities of *Ba*CDA and *Bl*CDA on chitin remains uncharacterized; however, their high hydrophobic scores and low S/V ratios suggest potential catalytic capability toward chitin substrates. Among the CDAs studied, *An*CDA, *As*CDA, *Ba*CDA, and *Sc*CDA exhibited distinct structural properties: *An*CDA contained conserved motifs with low hydrophobicity and a high S/V ratio, *Sc*CDA featured conserved motifs with high hydrophobicity and a low S/V ratio, while *As*CDA and *Ba*CDA displayed non-conserved motifs accompanied by high hydrophobicity and low S/V ratios. To investigate how

pocket architecture influences chitin deacetylation, these four enzymes were selected for heterologous expression and subsequent functional analysis.

Table 2. Properties and functional roles of CDAs active pockets.

Name	Hydrophobicity Score	Volume [Å^3]	Surface Area [Å^2]	Surface-to-Volume (S/V) Ratio	Substrate and the Removed Acetyl Group (%)
*As*CDA	37.933	172.130	391.39	2.274	Chitin (63%)
*Bl*CDA	23.923	150.020	317.250	2.115	Glycol chitin
*Bat*CDA	25.867	152.288	355.315	2.333	Colloidal chitin (44%)
*Ba*CDA	31.375	142.096	300.068	2.112	Glycol chitin
*Ar*CE4	11.583	151.550	344.330	2.272	Chitin(8%)
*Ar*CDA	10.300	135.170	307.300	2.273	β-chitin (2.99U/mg)
*Pa*CDA	11.750	154.624	356.668	2.307	Chitin (3%)
*Rc*CDA	25.250	121.860	329.730	2.706	Glycol chitin, no activity against chitin
*Cl*CDA	21.571	152.576	363.734	2.384	/
*Mr*CDA	16.231	139.780	368.790	2.638	Glycol chitin
*Rn*CDA	23.471	177.660	423.640	2.385	Glycol chitin
*Pes*CDA	18.538	154.624	358.381	2.318	Colloidal chitin (7%)
*Cc*CDA	9.750	148.480	354.772	2.389	No activity against chitin
*An*CDA	9.077	123.900	339.230	2.738	Chitin (0.5%)
*Rs*CDA	22.818	112.640	262.530	2.331	Colloidal chitin (27.5%)
*Sb*CDA	27.750	150.530	375.170	2.492	Colloidal chitin, no activity against chitin
*Sg*CDA	17.182	101.410	223.190	2.201	Colloidal chitin
*Sc*CDA	16.182	112.640	296.820	2.280	Shrimp shell chitin (11%)
*Ang*CDA	6.923	132.100	346.600	2.624	No activity against chitin
*Fv*CDA	10.846	118.272	286.080	2.419	Glycol chitin
*Af*CDA	8.750	144.380	332.850	2.305	Glycol chitin
*Pgt*CDA	21.733	112.130	292.240	2.606	No activity against chitin

3.2. Heterologous Expression and Purification of Recombinant CDAs

We constructed four recombinant strains of *E. coli* BL21(DE3), each carrying a pET-28a(+) expression vector encoding *An*CDA, *As*CDA, *Ba*CDA, or *Sc*CDA. After harvest and purification, the purity and molecular masses of the recombinant proteins were assessed by SDS–PAGE (Figure 4). The observed molecular weights of *An*CDA, *As*CDA, *Ba*CDA, and *Sc*CDA were 26.5 kDa, 42 kDa, 29 kDa, and 33 kDa, respectively, which were consistent with the predicted values (https://web.expasy.org/protparam/, accessed on 24 May 2024).

3.3. Optimal Reaction Conditions for Recombinant CDAs

To investigate the optimal reaction conditions of the four chitin deacetylases, we determined their thermal stability and pH stability. The results showed that different recombinant CDAs exhibited differences in their optimal stability conditions (Figures 5 and 6). In terms of thermal stability, *An*CDA performed best at 30 °C, retaining over 60% of its activity after 12 h of incubation. *Sc*CDA exhibited good stability within the temperature range of 30 °C. In contrast, *As*CDA and *Ba*CDA were more stable at 20–25 °C, with significant activity loss observed at temperatures exceeding 30 °C.

Regarding pH stability, *As*CDA, *An*CDA, *Ba*CDA, and *Sc*CDA showed high activity in phosphate buffer solutions within a pH range of 7.0–8.0, particularly near their respective optimal pH values.

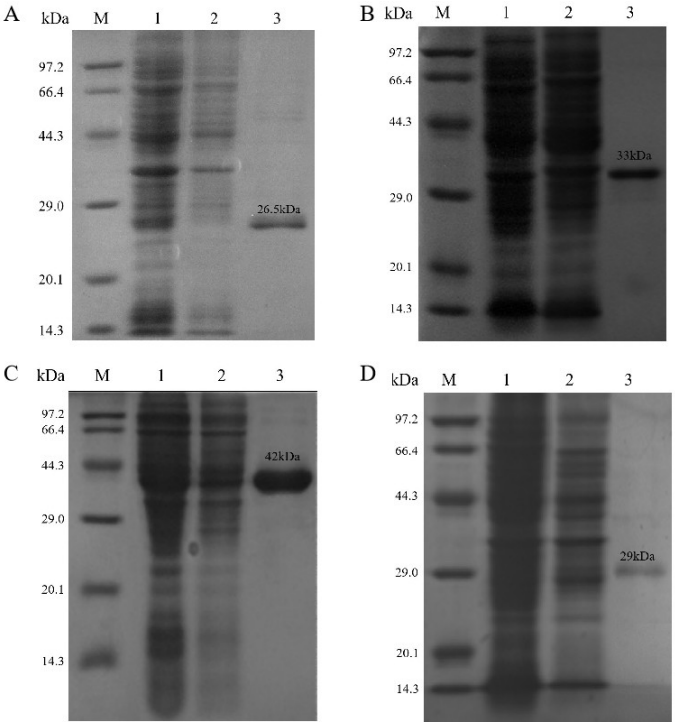


Figure 4. Results of SDS-PAGE analysis of (**A**) *An*CDA, (**B**) *Sc*CDA, (**C**) *As*CDA, and (**D**) *Ba*CDA. Lane 1 contains the crude enzyme solution of the recombinant protein; Lane 2 contains the flow-through collected during the low-imidazole equilibration phase of nickel column affinity chromatography; Lane 3 contains the purified recombinant protein collected during the high-imidazole elution phase of nickel column affinity chromatography.

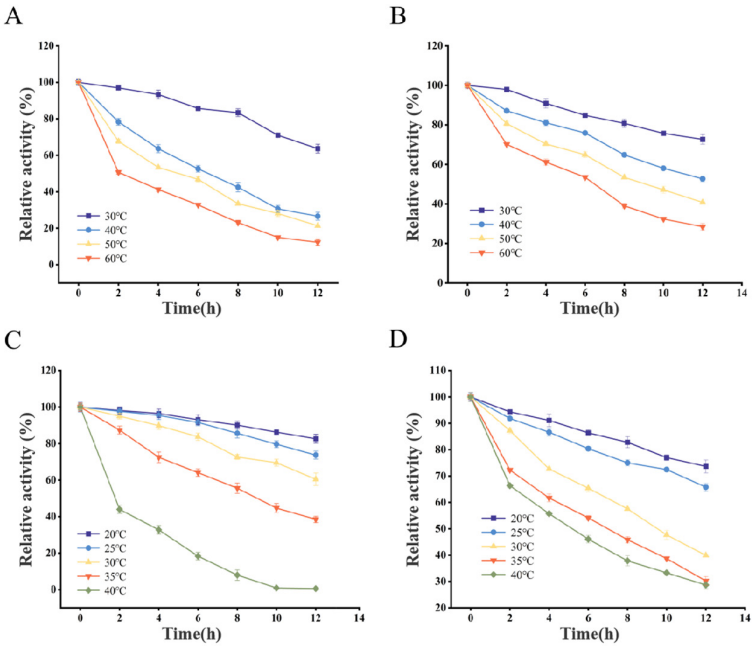


Figure 5. Temperature stability of *An*CDA (**A**), *Sc*CDA (**B**), *As*CDA (**C**), and *Ba*CDA (**D**).

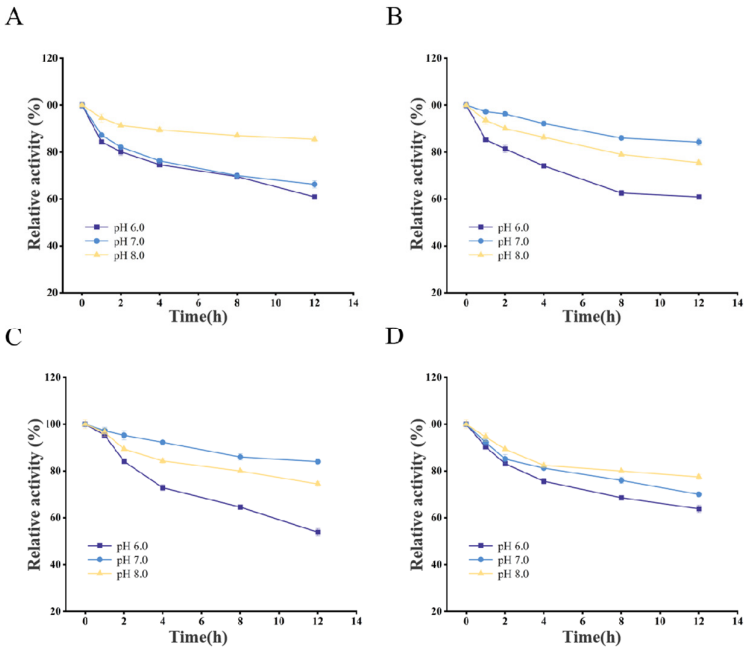


Figure 6. pH stability of *An*CDA (**A**), *As*CDA (**B**), *Ba*CDA (**C**), and *Sc*CDA (**D**).

Based on the aforementioned results, specific incubation parameters were defined to prevent suboptimal performance of the recombinant CDAs. The chosen conditions—phosphate buffer at 20 °C, pH 7.0 for *As*CDA and *Ba*CDA, and phosphate buffer at 30 °C, pH 8.0 for *An*CDA and *Sc*CDA—were thereby established for all subsequent work to ensure peak enzymatic function.

3.4. Recombinant Enzymes Process Chitin Substrates with Diverse Molecular Parameters

Substrates a–g, which possess distinct molecular parameters but comparable degrees of deacetylation and crystallinity, were prepared from commercial chitin. Their molecular parameters, degrees of deacetylation, and crystallinity were characterized using an Ubbelohde viscometer, FT-IR, and XRD analysis (Table 3).

Table 3. Physical and chemical parameters of chitin substrates and change in degree of deacetylation (ΔDD) after treatment with recombinant chitin deacetylases (*As*CDA, *An*CDA, *Ba*CDA, and *Sc*CDA).

Substrate	Molecular Weight (kDa)	Deacetylation (%)	Crystallinity (%)	*An*CDA (△DD)	*As*CDA (△DD)	*Ba*CDA (△DD)	*Sc*CDA (△DD)
Commercial chitin	563.42 ± 1.89	8.70 ± 2.66	76.49 ± 1.23	2.24 ± 0.50	33.47 ± 1.44	21.52 ± 1.03	7.41 ± 0.81
Substrate a	346.74 ± 3.12	18.06 ± 1.18	79.97 ± 1.87	3.10 ± 0.44	38.26 ± 0.68	25.43 ± 0.92	14.08 ± 0.96
Substrate b	322.67 ± 4.23	19.21 ± 0.92	73.97 ± 1.35	3.19 ± 0.92	37.32 ± 0.97	28.66 ± 0.87	16.37 ± 1.28
Substrate c	278.72 ± 2.38	19.35 ± 0.78	78.78 ± 1.87	5.84 ± 2.66	42.93 ± 1.21	29.88 ± 1.24	21.77 ± 0.79
Substrate d	164.40 ± 5.23	16.19 ± 0.89	80.03 ± 2.01	9.11 ± 0.89	47.58 ± 1.04	34.41 ± 1.03	20.44 ± 0.84
Substrate e	64.80 ± 1.98	16.99 ± 1.21	76.00 ± 1.48	16.42 ± 1.20	52.46 ± 0.91	37.57 ± 1.23	30.45 ± 1.18
Substrate f	33.36 ± 2.23	16.70 ± 0.93	81.07 ± 1.29	21.51 ± 1.03	49.49 ± 1.23	35.57 ± 1.27	28.48 ± 1.21
Substrate g	14.46 ± 3.68	19.72 ± 1.37	77.14 ± 0.89	28.43 ± 1.30	59.54 ± 1.53	49.08 ± 1.34	42.18 ± 1.68

Functional group absorption profiles were examined by FT-IR spectroscopy. Variations in the degree of deacetylation modulate intermolecular and intramolecular hydrogen bonding of amide groups, leading to band shifts in the spectra. FT-IR data were used to quantify the degree of deacetylation (Figure 7a). In the spectra, the bands at 1662 and 1627 cm^{-1} correspond to amide I (C=O stretching, intra-chain N–H and inter-chain O–H hydrogen bonds); the 1561 cm^{-1} band reflects N–H bending (amide II); and the

1315–1320 cm^{-1} band arises from C–N bending (amide III) [35,52]. Naturalchitin exhibits high crystallinity. Wide-angle XRD was employed to record diffraction intensities and calculate crystallinity indices based on reflections at 2θ = 9–10° and 2θ = 19–20° (Figure 7b). Commercial α-chitin displayed two characteristic peaks at approximately 9.3° and 19.2°, assigned to the (020) and (110) crystal planes, respectively [53]. In contrast, sample 9 (chitosan) lacked the (020) reflection, whereas samples 1–8 retained both chitin peaks.

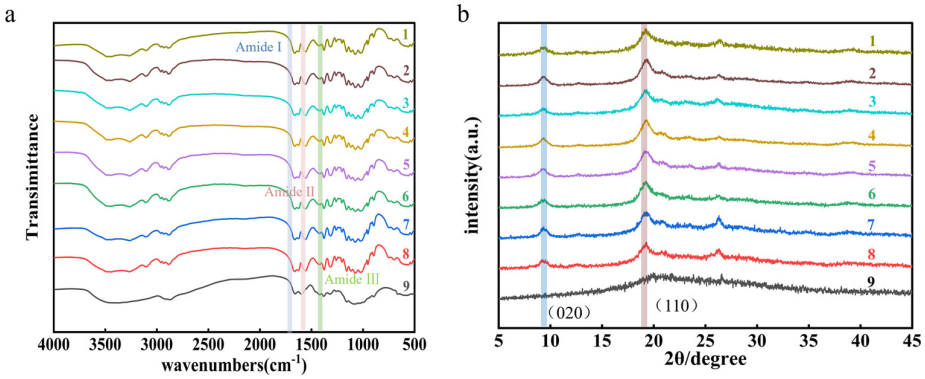


Figure 7. (**a**) Fourier transform infrared spectra and (**b**) X-ray diffraction patterns of chitin and chitosan samples. Sample 1 is commercial chitin, samples 2–8 are substrates a–g, and sample 9 is commercial chitosan.

Enzymatic deacetylation assays were performed using *As*CDA, *An*CDA, *Ba*CDA, and *Sc*CDA on commercial chitin and substrates a–g. The DD of the reaction products was determined by FT-IR, and enzyme performance was quantified as the change in DD (ΔDD) (Table 3) compared to untreated substrates.

*An*CDA, characterized by low hydrophobicity and a high S/V ratio, demonstrated limited deacetylation efficiency toward high-molecular-weight chitin (2.24% acetyl removal for 563 kDa), but effectively catalyzed low-molecular-weight substrates, achieving 28.43% deacetylation for 14 kDa chitin. *Sc*CDA, with higher hydrophobicity and a lower S/V ratio, exhibited moderate activity on 563 kDa chitin (7.41% deacetylation), though its preference for smaller substrates remained predominant. Both fungal-derived *An*CDA and *Sc*CDA feature conserved MT1–MT5 motifs and negatively charged active pockets, which stabilize metal ions and catalytic residues. However, their restricted pocket volume and shallow architecture likely hinder full access of bulky, crystalline chitin chains to the catalytic site.

In contrast, *As*CDA and *Ba*CDA, which exhibited high hydrophobicity and low S/V ratios, displayed superior deacetylation efficiencies toward high-molecular-weight chitin (33.47% and 21.52% acetyl removal for 563 kDa, respectively), in alignment with their structural profiles. Notably, *As*CDA's expanded binding pocket accommodates larger substrate volumes, while its hydrophobic-rich interior facilitates interactions with the non-polar regions of chitin, collectively enhancing catalytic performance. These experimental results indicate that the critical roles of pocket hydrophobicity, geometry, and accessibility in determining substrate specificity.

4. Conclusions

For the first time, this study integrates phylogenetic analysis, multiple sequence alignment, structural prediction (AlphaFold3), and computer-aided tools to conduct extensive analysis and summarization of the physicochemical properties and catalytic capabilities of the active pockets of CDAs, thereby providing a theoretical basis and technical pathway for the discovery of new enzymes. By integrating computational modeling and functional validation, we demonstrated that conserved fungal enzymes (such as AnCDA and ScCDA) exhibited a preference for low-molecular-weight substrates, which reflected their biolog-

ical functions in cell wall remodeling. In contrast, enzymes with high hydrophobicity and low S/V ratios (such as AsCDA and BaCDA) demonstrated higher efficiency in the deacetylation of high-molecular-weight crystalline chitin. These enzymes utilized non-canonical motifs and optimized pocket structures to overcome substrate rigidity, thereby breaking through the bottleneck faced by most fungal CDAs. Shallow pockets and high hydrophobic scores significantly enhanced the affinity for crystalline chitin, providing new perspectives on the functional evolution of non-conserved motif enzymes and offering theoretical foundations and technical pathways for the discovery of new enzymes and protein engineering.

However, this study still has certain limitations: (1) Although our study provides some fundamental insights, through structural models predicted by AlphaFold 3, the activity of enzymes on crystalline substrates may also depend on transient structural dynamics. For example, the low S/V ratio of BaCDA may facilitate an induced-fit mechanism during substrate binding, a hypothesis that can be validated through molecular dynamics simulations. (2) This study only explored regulation of the molecular weight of substrates and did not explore substrates with different degrees of deacetylation, and further investigation into the substrate spectra of different CDAs is required. (3) Additionally, this study found that the pocket of BaCDA contains arginine residues, and how this positive charge affects substrate binding when ionic strength changes has not yet been clarified, necessitating exploration through subsequent mutation experiments. Future research should explore how pocket flexibility or allosteric regulation fine-tunes enzyme activity under industrial conditions, such as high substrate concentrations and elevated ionic strength.

Author Contributions: Investigation, data curation, methodology, software, writing—original draft, K.C.; Data curation and methodology, S.Y.; funding acquisition and review and Editing, J.C. All authors have read and agreed to the published version of the manuscript.

Funding: This work was supported by funding from the Key Laboratory of Fermentation Engineering (Ministry of Education) (202209FE07) and the Key R&D projects in Hubei Province (2022BBA0053).

Institutional Review Board Statement: Not applicable.

Informed Consent Statement: Not applicable.

Data Availability Statement: The original contributions presented in this study are included in the article. Further inquiries can be directed to the corresponding author.

Acknowledgments: The authors express their gratitude to the Key Laboratory of Fermentation Engineering (Ministry of Education), School of Life and Health Sciences, Hubei University of Technology, for its support.

Conflicts of Interest: We declare that we have no known competing financial interests or personal relationships that could have appeared to influence the work reported in this paper.

Abbreviations

The following abbreviations are used in this manuscript:

CDA	Chitin deacetylase
DD	Degree of deacetylation
GlcNAc	N-Acetyl-D-glucosamine
MT1–MT5	Motif 1–motif5
△DD	Percentage of acetyls removed

References

1. Kim, S.-K. *Chitin, Chitosan, Oligosaccharides and Their Derivatives: Biological Activities and Applications*; CRC Press: Boca Raton, FL, USA, 2010. [CrossRef]
2. Mohan, K.; Ganesan, A.R.; Ezhilarasi, P.; Kondamareddy, K.K.; Rajan, D.K.; Sathishkumar, P.; Rajarajeswaran, J.; Conterno, L. Green and eco-friendly approaches for the extraction of chitin and chitosan: A review. *Carbohydr. Polym.* **2022**, *287*, 119349. [CrossRef]
3. Xu, Y.; Han, J.; Lin, H. Fabrication and characterization of a self-crosslinking chitosan hydrogel under mild conditions without the use of strong bases. *Carbohydr. Polym.* **2017**, *156*, 372–379. [CrossRef]
4. Gonçalves, C.; Ferreira, N.; Lourenço, L. Production of low molecular weight chitosan and chitooligosaccharides (COS): A review. *Polymers* **2021**, *13*, 2466. [CrossRef] [PubMed]
5. Pan, H.; Zhao, T.; Xu, L.; Shen, Y.; Wang, L.; Ding, Y. Preparation of novel chitosan derivatives and applications in functional finishing of textiles. *Int. J. Biol. Macromol.* **2020**, *153*, 971–976. [CrossRef] [PubMed]
6. Friedman, M.; Juneja, V.K. Review of antimicrobial and antioxidative activities of chitosans in food. *J. Food Prot.* **2010**, *73*, 1737–1761. [CrossRef]
7. Lin, S.; Qin, Z.; Chen, Q.; Fan, L.; Zhou, J.; Zhao, L. Efficient immobilization of bacterial GH family 46 chitosanase by carbohydrate-binding module fusion for the controllable preparation of chitooligosaccharides. *J. Agric. Food. Chem.* **2019**, *67*, 6847–6855. [CrossRef]
8. Pokhrel, S.; Yadav, P.N. Functionalization of chitosan polymer and their applications. *J. Macromol. Sci. Part A* **2019**, *56*, 450–475. [CrossRef]
9. El Knidri, H.; El Khalfaouy, R.; Laajeb, A.; Addaou, A.; Lahsini, A. Eco-friendly extraction and characterization of chitin and chitosan from the shrimp shell waste via microwave irradiation. *Process Saf. Environ. Prot.* **2016**, *104*, 395–405. [CrossRef]
10. Nawaz, H.; Mannan, R.; Nishan, U. Modification of physical and functional characteristics of chitin extracted from microwave-treated Nelumbo nucifera rhizome flour. *Polym. Polym. Compos.* **2021**, *29*, S1257–S1267. [CrossRef]
11. Giraldo, J.D.; García, Y.; Vera, M.; Garrido-Miranda, K.A.; Andrade-Acuna, D.; Marrugo, K.P.; Rivas, B.L.; Schoebitz, M. Alternative processes to produce chitin, chitosan, and their oligomers. *Carbohydr. Polym.* **2024**, *332*, 121924. [CrossRef]
12. Hossbach, J.; Busswinkel, F.; Kranz, A.; Wattjes, J.; Cord-Landwehr, S.; Moerschbacher, B.M. A chitin deacetylase of Podospora anserina has two functional chitin binding domains and a unique mode of action. *Carbohydr. Polym.* **2018**, *183*, 1–10. [CrossRef]
13. Qing, L.; Gao, J.; Du, L.; Liu, Y.; Guo, N.; Sun, J.; Dong, H.; Mao, X. Chitinase and deacetylase-based chitin-degrading bacteria: One-pot cascade bioconversion of chitin to chitooligosaccharides. *J. Agric. Food. Chem.* **2024**, *72*, 23937–23946. [CrossRef] [PubMed]
14. Liang, B.; Song, W.; Xing, R.; Liu, S.; Yu, H.; Li, P. The source, activity influencing factors and biological activities for future development of chitin deacetylase. *Carbohydr. Polym.* **2023**, *321*, 121335. [CrossRef]
15. Naqvi, S.; Moerschbacher, B.M. The cell factory approach toward biotechnological production of high-value chitosan oligomers and their derivatives: An update. *Crit. Rev. Biotechnol.* **2017**, *37*, 11–25. [CrossRef] [PubMed]
16. Kaczmarek, M.B.; Struszczyk-Swita, K.; Xiao, M.; Szczęsna-Antczak, M.; Antczak, T.; Gierszewska, M.; Steinbüchel, A.; Daroch, M. Polycistronic expression system for Pichia pastoris composed of chitino-and chitosanolytic enzymes. *Front. Bioeng. Biotechnol.* **2021**, *9*, 710922. [CrossRef] [PubMed]
17. Aragunde, H.; Biarnés, X.; Planas, A. Substrate recognition and specificity of chitin deacetylases and related family 4 carbohydrate esterases. *Int. J. Mol. Sci.* **2018**, *19*, 412. [CrossRef]
18. Lindner, S.; Bonin, M.; Hellmann, M.J.; Moerschbacher, B.M. Three intertwining effects guide the mode of action of chitin deacetylase de-and N-acetylation reactions. *Carbohydr. Polym.* **2025**, *347*, 122725. [CrossRef]
19. Blair, D.E.; Schüttelkopf, A.W.; MacRae, J.I.; van Aalten, D.M. Structure and metal-dependent mechanism of peptidoglycan deacetylase, a streptococcal virulence factor. *Proc. Natl. Acad. Sci. USA* **2005**, *102*, 15429–15434. [CrossRef]
20. Blair, D.E.; Hekmat, O.; Schüttelkopf, A.W.; Shrestha, B.; Tokuyasu, K.; Withers, S.G.; van Aalten, D.M. Structure and mechanism of chitin deacetylase from the fungal pathogen *Colletotrichum lindemuthianum*. *Biochemistry* **2006**, *45*, 9416–9426. [CrossRef]
21. Nakamura, A.M.; Nascimento, A.S.; Polikarpov, I. Structural diversity of carbohydrate esterases. *Biotechnol. Res. Innov.* **2017**, *1*, 35–51. [CrossRef]
22. Mapuranga, J.; Chang, J.; Li, H.; Zhang, Y.; Li, R.; Song, L.; Zhang, N.; Yang, W. The molecular structure, biological roles, and inhibition of plant pathogenic fungal chitin deacetylases. *Front. Plant Sci.* **2024**, *14*, 1335646. [CrossRef]
23. Yang, X.; Gao, H.; Yan, J.; Zhou, J.; Shi, L. Intramolecular chaperone-assisted dual-anchoring activation (ICDA): A suitable preorganization for electrophilic halocyclization. *Chem. Sci.* **2024**, *15*, 6130–6140. [CrossRef]
24. Taher, M.; Dubey, K.D.; Mazumdar, S. Computationally guided bioengineering of the active site, substrate access pathway, and water channels of thermostable cytochrome P450, CYP175A1, for catalyzing the alkane hydroxylation reaction. *Chem. Sci.* **2023**, *14*, 14316–14326. [CrossRef]

25. Nie, Y.; Wang, S.; Xu, Y.; Luo, S.; Zhao, Y.; Xiao, R.; Montelione, G.; Hunt, J.; Szyperski, T. Enzyme engineering based on X-ray structures and kinetic profiling of substrate libraries: Alcohol dehydrogenases for stereospecific synthesis of a broad range of chiral alcohols. *ACS Catal.* **2018**, *8*, 5145–5152. [CrossRef]
26. Waterhouse, A.M.; Procter, J.B.; Martin, D.M.; Clamp, M.; Barton, G.J. Jalview Version 2—A multiple sequence alignment editor and analysis workbench. *Bioinformatics* **2009**, *25*, 1189–1191. [CrossRef] [PubMed]
27. Tamura, K.; Stecher, G.; Kumar, S. MEGA11: Molecular evolutionary genetics analysis version 11. *Mol. Biol. Evol.* **2021**, *38*, 3022–3027. [CrossRef] [PubMed]
28. Abramson, J.; Adler, J.; Dunger, J.; Evans, R.; Green, T.; Pritzel, A.; Ronneberger, O.; Willmore, L.; Ballard, A.J.; Bambrick, J. Accurate structure prediction of biomolecular interactions with AlphaFold 3. *Nature* **2024**, *630*, 493–500. [CrossRef]
29. Jurrus, E.; Engel, D.; Star, K.; Monson, K.; Brandi, J.; Felberg, L.E.; Brookes, D.H.; Wilson, L.; Chen, J.; Liles, K. Improvements to the APBS biomolecular solvation software suite. *Protein Sci.* **2018**, *27*, 112–128. [CrossRef]
30. Graef, J.; Ehrt, C.; Rarey, M. Binding site detection remastered: Enabling fast, robust, and reliable binding site detection and descriptor calculation with DoGSite3. *J. Chem. Inf. Model.* **2023**, *63*, 3128–3137. [CrossRef] [PubMed]
31. Schmidtke, P.; Le Guilloux, V.; Maupetit, J.; Tufféry, P. Fpocket: Online tools for protein ensemble pocket detection and tracking. *Nucleic Acids Res.* **2010**, *38*, W582–W589. [CrossRef]
32. Sun, Y.; Zhang, J.; Wu, S.; Wang, S. Statistical optimization for production of chitin deacetylase from *Rhodococcus erythropolis* HG05. *Carbohydr. Polym.* **2014**, *102*, 649–652. [CrossRef]
33. Delezuk, J.A.d.M.; Cardoso, M.B.; Domard, A.; Campana-Filho, S.P. Ultrasound-assisted deacetylation of beta-chitin: Influence of processing parameters. *Polym. Int.* **2011**, *60*, 903–909. [CrossRef]
34. Poirier, M.; Charlet, G. Chitin fractionation and characterization in N, N-dimethylacetamide/lithium chloride solvent system. *Carbohydr. Polym.* **2002**, *50*, 363–370. [CrossRef]
35. Kasaai, M.R. A review of several reported procedures to determine the degree of N-acetylation for chitin and chitosan using infrared spectroscopy. *Carbohydr. Polym.* **2008**, *71*, 497–508. [CrossRef]
36. Kenawy, E.-R.; Ali, S.S.; Al-Etewy, M.; Sun, J.; Wu, J.; El-Zawawy, N. Synthesis, characterization and biomedical applications of a novel Schiff base on methyl acrylate-functionalized chitosan bearing p-nitrobenzaldehyde groups. *Int. J. Biol. Macromol.* **2019**, *122*, 833–843. [CrossRef] [PubMed]
37. Xiao, M.; Chen, D.; Liu, S.; Chen, A.; Fang, A.; Tian, B.; Yu, Y.; Bi, C.; Kang, Z.; Yang, Y. A chitin deacetylase Ps CDA2 from *Puccinia striiformis* f. sp. tritici confers disease pathogenicity by suppressing chitin-triggered immunity in wheat. *Mol. Plant Pathol.* **2023**, *24*, 1467–1479. [CrossRef] [PubMed]
38. Christodoulidou, A.; Bouriotis, V.; Thireos, G. Two sporulation-specific chitin deacetylase-encoding genes are required for the ascospore wall rigidity of *Saccharomyces cerevisiae*. *J. Biol. Chem.* **1996**, *271*, 31420–31425. [CrossRef] [PubMed]
39. Davis, L.L.; Bartnicki-Garcia, S. Chitosan synthesis by the tandem action of chitin synthetase and chitin deacetylase from *Mucor rouxii*. *Biochemistry* **1984**, *23*, 1065–1073. [CrossRef]
40. Tsigos, I.; Martinou, A.; Kafetzopoulos, D.; Bouriotis, V. Chitin deacetylases: New, versatile tools in biotechnology. *Trends Biotechnol.* **2000**, *18*, 305–312. [CrossRef]
41. Pawaskar, G.M.; Raval, K.; Rohit, P.; Shenoy, R.P.; Raval, R. Cloning, expression, purification and characterization of chitin deacetylase extremozyme from halophilic *Bacillus aryabhattai* B8W22. *3 Biotech* **2021**, *11*, 515. [CrossRef]
42. Zhao, Y.; Park, R.-D.; Muzzarelli, R.A. Chitin deacetylases: Properties and applications. *Mar. Drugs* **2010**, *8*, 24–46. [CrossRef] [PubMed]
43. Tuveng, T.R.; Rothweiler, U.; Udatha, G.; Vaaje-Kolstad, G.; Smalås, A.; Eijsink, V.G. Structure and function of a CE4 deacetylase isolated from a marine environment. *PLoS ONE* **2017**, *12*, e0187544. [CrossRef]
44. Yamada, M.; Kurano, M.; Inatomi, S.; Taguchi, G.; Okazaki, M.; Shimosaka, M. Isolation and characterization of a gene coding for chitin deacetylase specifically expressed during fruiting body development in the basidiomycete *Flammulina velutipes* and its expression in the yeast Pichia pastoris. *FEMS Microbiol. Lett.* **2008**, *289*, 130–137. [CrossRef]
45. Geoghegan, I.A.; Gurr, S.J. Chitosan mediates germling adhesion in *Magnaporthe oryzae* and is required for surface sensing and germling morphogenesis. *PLoS Pathog.* **2016**, *12*, e1005703. [CrossRef]
46. Yang, G.; Wang, Y.; Fang, Y.; An, J.; Hou, X.; Lu, J.; Zhu, R.; Liu, S. A novel potent crystalline chitin decomposer: Chitin deacetylase from *Acinetobacter schindleri* MCDA01. *Molecules* **2022**, *27*, 5345. [CrossRef]
47. Abd El-Ghany, M.N.; Hamdi, S.A.; Zahran, A.K.; Abou-Taleb, M.A.; Heikel, A.M.; Abou El-Kheir, M.T.; Farahat, M.G. Characterization of novel cold-active chitin deacetylase for green production of bioactive chitosan. *AMB Express* **2025**, *15*, 5. [CrossRef]
48. Zhu, X.-Y.; Zhao, Y.; Zhang, H.-D.; Wang, W.-X.; Cong, H.-H.; Yin, H. Characterization of the specific mode of action of a chitin deacetylase and separation of the partially acetylated chitosan oligosaccharides. *Mar. Drugs* **2019**, *17*, 74. [CrossRef] [PubMed]
49. Liu, Z.; Gay, L.M.; Tuveng, T.R.; Agger, J.W.; Westereng, B.; Mathiesen, G.; Horn, S.J.; Vaaje-Kolstad, G.; Van Aalten, D.M.; Eijsink, V.G. Structure and function of a broad-specificity chitin deacetylase from *Aspergillus nidulans* FGSC A4. *Sci. Rep.* **2017**, *7*, 1746. [CrossRef]

50. Wujieti, B.; Feng, X.; Liu, E.; Li, D.; Hao, M.; Zhou, L.; Cui, W. A theoretical study on the activity and selectivity of IDO/TDO inhibitors. *Phys. Chem. Chem. Phys.* **2024**, *26*, 16747–16764. [CrossRef]
51. Distaso, M.; Cea-Rama, I.; Coscolín, C.; Chernikova, T.N.; Tran, H.; Ferrer, M.; Sanz-Aparicio, J.; Golyshin, P.N. The mobility of the cap domain is essential for the substrate promiscuity of a family IV esterase from sorghum rhizosphere microbiome. *Appl. Environ. Microbiol.* **2023**, *89*, e01807–e01822. [CrossRef] [PubMed]
52. Qin, C.; Li, H.; Xiao, Q.; Liu, Y.; Zhu, J.; Du, Y. Water-solubility of chitosan and its antimicrobial activity. *Carbohydr. Polym.* **2006**, *63*, 367–374. [CrossRef]
53. Li, K.; Liang, Y.; Fang, J.; Peng, J.; Tan, M. Chitin deacetylase from *Bacillus aryabhattai* TCI-16: Heterologous expression, characterization, and deacetylation performance. *J. Agric. Food Chem.* **2024**, *72*, 9268–9278. [CrossRef] [PubMed]

Disclaimer/Publisher's Note: The statements, opinions and data contained in all publications are solely those of the individual author(s) and contributor(s) and not of MDPI and/or the editor(s). MDPI and/or the editor(s) disclaim responsibility for any injury to people or property resulting from any ideas, methods, instructions or products referred to in the content.